Am J Nucl Med Mol Imaging 2013;3(1):71-84
www.ajnmmi.us /ISSN:2160-8407/ajnmmi1209003

*Original Article*

# Synthesis and preclinical evaluation of a new C-6 alkylated pyrimidine derivative as a PET imaging agent for HSV1-*tk* gene expression

Ursina Müller[1], Tobias L Ross[1], Charlene Ranadheera[1], Roger Slavik[1], Adrienne Müller[1], Mariana Born[1], Evelyn Trauffer[1], Selena Milicevic Sephton[1], Leonardo Scapozza[2], Stefanie D Krämer[1], Simon M Ametamey[1]

*[1]Institute of Pharmaceutical Sciences, ETH Zurich, Wolfgang-Pauli Strasse 10, 8093 Zurich, Switzerland; [2]University of Geneva, School of Pharmaceutical Sciences, Quai Ernest-Ansermet 30, 1211 Geneva 4, Switzerland*

Received September 27, 2012; Accepted November 2, 2012; Epub January 5, 2013; Published January 15, 2013

**Abstract:** [$^{18}$F]FHOMP (6-((1-[$^{18}$F]-fluoro-3-hydroxypropan-2-yloxy)methyl)-5-methylpyrimidine-2,4(1*H*,3*H*)-dione), a C-6 substituted pyrimidine derivative, has been synthesized and evaluated as a potential PET agent for imaging herpes simplex virus type 1 thymidine kinase (HSV1-*tk*) gene expression. [$^{18}$F]FHOMP was prepared by the reaction of the tosylated precursor with tetrabutylammonium [$^{18}$F]-fluoride followed by acidic cleavage of the protecting groups. *In vitro* cell accumulation of [$^{18}$F]FHOMP and [$^{18}$F]FHBG (reference) was studied with HSV1-*tk* transfected HEK293 (HEK293TK+) cells. Small animal PET and biodistribution studies were performed with HEK293TK+ xenograft-bearing nude mice. The role of equilibrative nucleoside transporter 1 (ENT1) in the transport and uptake of [$^{18}$F]FHOMP was also examined in nude mice after treatment with ENT1 inhibitor nitrobenzylmercaptopurine ribonucleoside phosphate (NBMPR-P). [$^{18}$F]FHOMP was obtained in a radiochemical yield of ~25% (decay corrected) and the radiochemical purity was greater than 95%. The uptake of [$^{18}$F]FHOMP in HSV1-TK containing HEK293TK+ cells was 52 times (at 30 min) and 244 times (at 180 min) higher than in control HEK293 cells. The uptake ratios between HEK293TK+ and HEK293 control cells for [$^{18}$F]FHBG were significantly lower i.e. 5 (at 30 min) and 81 (240 min). *In vivo*, [$^{18}$F]FHOMP accumulated to a similar extend in HEK293TK+ xenografts as [$^{18}$F]FHBG but with a higher general background. Blocking of ENT1 reduced [$^{18}$F]FHOMP uptake into brain from a standardized uptake value (SUV) of 0.10±0.01 to 0.06±0.02, but did not reduce the general background signal in PET. Although [$^{18}$F]FHOMP does not outperform [$^{18}$F]FHBG in its *in vivo* performance, this novel C-6 pyrimidine derivative may be a useful probe for monitoring HSV1-*tk* gene expression *in vivo*.

**Keywords:** HSV1-TK, reporter gene, gene expression monitoring, PET, [$^{18}$F]FHOMP, [$^{18}$F]FHBG

## Introduction

Reporter gene imaging with positron emission tomography (PET) is a powerful non-invasive tool to study different biological processes in preclinical settings and currently offers a great potential for translation into the clinic.. It allows for monitoring different molecular cellular processes such as transcriptional regulation, protein-protein interactions, cell targeting and cell trafficking of e.g. immune cell, cancer cells or stem cells and targeted drug action [1]. The gene encoding herpes simplex virus type 1 thymidine kinase (HSV1-*tk*) is commonly used as a reporter gene in preclinical studies in combination with small animal PET. Uptake into cells of a PET reporter probe followed by selective phosphorylation by HSV1-TK leads to metabolic trapping of the radiotracer in HSV1-TK expressing cells, thus providing indirect information about the location, extent and duration of expression of the gene of interest. Several nucleoside analogs that are selectively phosphorylated by HSV1-TK have been synthesized [2, 3].

Nucleosides are transported into cells mainly via two types of transporters: the concentrative (CNT, SLC28) and equilibrative (ENT, SLC29) nucleoside transporters. Besides providing uptake into the cells of interest, these transporters can have an impact on the general bio-

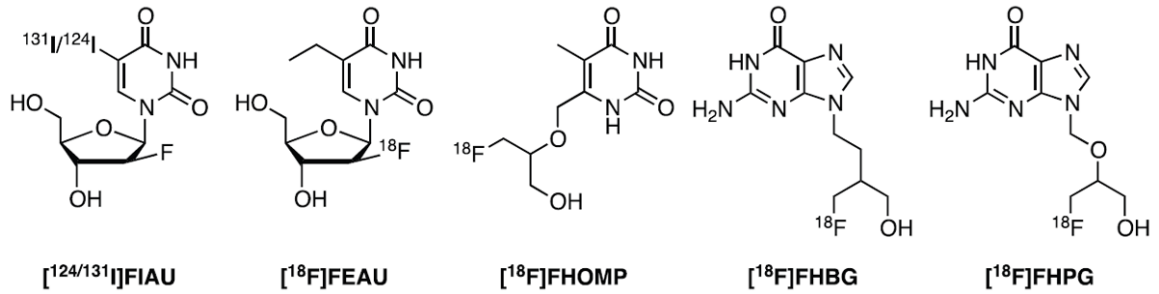


**Figure 1.** Chemical structures of 5-[$^{124/131}$I]-2'-deoxy-2'-fluoro-1-β-D-arabino-uracil ([$^{124/131}$I]FIAU), 2'-deoxy-2'-[$^{18}$F]-fluoro-5-ethyl-1-β-D-arabinofuranosyl-uracil ([$^{18}$F]FEAU), 9-(4-[$^{18}$F]-fluoro-3-(hydroxymethyl)butyl)guanine ([$^{18}$F]FHBG), 9-((3-[$^{18}$F]fluoro-1-hydroxy-2-propoxy)-methyl)guanine ([$^{18}$F]FHPG) and 6-((1-[$^{18}$F]-fluoro-3-hydroxypropan-2-yloxy) methyl)-5-methylpyrimidine-2,4(1*H*,3*H*)-dione ([$^{18}$F]FHOMP).

distribution of nucleoside PET probes as recently shown for the mammalian thymidine kinase-1 (TK1) substrate 3'-deoxy-3'-[$^{18}$F]fluorothymidine [$^{18}$F]FLT and ENT1 [4].

HSV1-TK phosphorylates a broad range of nucleoside analogs and its expression can be imaged with several substrates including pyrimidine derivatives 5-[$^{124/131}$I]-2'-deoxy-2'-fluoro-1-β-D-arabino-uracil ([$^{124/131}$I]FIAU), 2'-deoxy-2'-[$^{18}$F]-fluoro-5-ethyl-1-β-D-arabinofuranosyl-uracil ([$^{18}$F]FEAU), or acycloguanosine derivatives, such as 9-(4-[$^{18}$F]-fluoro-3-[hydroxymethyl]butyl)guanine ([$^{18}$F]FHBG) (**Figure 1**) [5-9]. The high selectivity for viral over mammalian TK is a prerequisite for a good probe for HSV1-TK. FIAU is an example with suboptimal selectivity for HSV1-TK as it showed some accumulation in xenografts devoid of viral TK due to the phosphorylation by cellular TK1 [10]. FHBG on the other hand, exhibits high abdominal radioactivity concentrations due to hepatobiliary elimination. This makes tracking of the reporter gene close to the abdomen impossible. In addition, when compared to pyrimidines, FHBG is less sensitive towards the native HSV1-TK [10-12]. The development of a radiotracer with optimal distribution between HSV1-TK expressing cells and normal tissues remains an ambitious goal for reporter gene imaging.

In the search for improved PET radiotracers for HSV1-*tk* gene expression monitoring, we reported previously on a number of C-6 alkylated pyrimidine derivatives and showed that these new pyrimidine derivatives have high binding affinities for HSV1-TK and exhibit no cytotoxic effects [13, 14]. In this work, we report on the development and evaluation of 6-((1-fluoro-3-hydroxypropan-2-yloxy)methyl)-5-methylpyrimidine-2,4(1*H*,3*H*)-dione (FHOMP), a pyrimidine nucleoside substituted at the C-6 position with a side chain in analogy to the antiviral drug ganciclovir and the HSV1-TK PET tracer 9-((3-[$^{18}$F]fluoro-1-hydroxy-2-propoxy)-methyl)guanine [$^{18}$F]FHPG (**Figure 1**). We describe the synthesis of the non-radioactive reference compound and precursor as well as the radiosynthesis of [$^{18}$F]FHOMP using a two-step reaction sequence. The latter was achieved by N-1 protection of the precursor preventing intramolecular cyclization between N-1 and the acyclic moiety at C-6 during the radiosynthesis. We further report on the *in vitro* and *in vivo* evaluation of [$^{18}$F]FHOMP using HSV1-TK positive and control HEK293 (human embryonic kidney) cells, murine P388 control cells and HEK293TK+ xenograft-bearing nude mice. The well-established radiotracer, [$^{18}$F]FHBG, was used as reference for the biological evaluation. Furthermore, we investigated the effect of ENT1 inhibition on the biodistribution of [$^{18}$F]FHOMP. The transporter is expressed in many human, rat and mouse tissues [15-18] and may therefore influence the distribution of [$^{18}$F]FHOMP.

## Materials and methods

### *General*

All reagents and solvents were purchased from Sigma-Aldrich Chemie GmbH or VWR International AG. All chemicals were used as supplied unless stated otherwise. Dulbecco's modified Eagle's medium (DMEM+GlutaMAX-I) with a high glucose concentration (4.5 g/L) and pyruvate, trypsin 0.25% with EDTA, geneticine

(G418) and fetal bovine serum (FBS) were purchased from Gibco. The precursor, $N^2$-(*p*-Anisyldiphenylmethyl)-9-[(4-(*p*-toluolsulfonyloxy))-3-(*p*-anisyldiphenylmethoxymethyl)butyl]guanine (tosyl-FHBG), and the reference compound (9-(4-fluoro-3-[hydroxymethyl]butyl)guanine) were purchased from ABX GmbH, Germany. No-carrier-added aqueous [$^{18}$F]-fluoride ion was produced on an IBA Cyclone 18/9 cyclotron by irradiation of 2.0 mL water target (for a large volume target) or 0.585 mL (for a small volume target) using a 18 MeV proton beam on 98% enriched [$^{18}$O]water using the $^{18}O(p,n)^{18}F$ nuclear reaction. No-carrier added [$^{18}$F]-fluoride (~28-86 GBq) was trapped on an anion exchange cartridge (Sep-Pak Light Accell Plus QMA; Waters AG), preconditioned with 5 mL of aqueous 0.5 M potassium carbonate solution and 5 mL of water. [$^{18}$F]FHBG was prepared as previously reported [19].

*Cell line and transfection*

HEK293 human embryonic kidney cells were obtained from the Leibniz Institute DSMZ-German Collection of Microorganisms and Cell Cultures (Braunschweig, Germany). HEK293 is a transformed cell line (sheared adenovirus 5 DNA) and can thus form xenografts. The P388 murine leukemia cells were obtained from the Japan Health Science Research Resources Bank (Osaka, Japan). HEK293 cells were stably transfected with a plasmid encoding the wild-type HSV1-*tk* gene (HEK293TK+ cells). In addition to the HSV1-*tk* gene, the plasmid contained a red fluorescent protein (*RFP*) gene, and G418 resistance gene. The plasmid was kindly provided by Prof. Sanjiv Sam Gambhir, Department of Radiology – Nuclear Medicine, Stanford University, Palo Alto CA, USA. Plasmid DNA was linearized by digestion using the restriction enzyme BglII (10 u/μL, Promega) at 37 °C overnight and was subsequently purified using the QIAquick Purification Kit (Qiagen) as recommended by the manufacturer. The linearized DNA was transfected into 60-80% confluent HEK293 cells using Lipofectamine 2000 (Invitrogen) as recommended by the manufacturer. The transfection medium was removed after 24 hours and replaced with DMEM+GlutaMAX-I medium supplemented with 10% FBS and G418 (300 μg/mL) to select for the HSV-*tk* transgenic cells. Cells were detached with trypsin/EDTA (Invitrogen) and stocks were frozen in liquid nitrogen. Resuscitated cells were used for a maximum of 10 passages. HSV1-TK expression was verified indirectly by visualizing the RFP by flow cytometry on a FACSCalibur (BD Biosciences) immediately after transfection and by fluorescent microscopy after freezing and resuscitation of the cells. In flow cytometry, 71% of transfected cultures were positive for the transgene. In fluorescence microscopy, resuscitated HEK293TK+ cells showed a strong signal at the respective wavelength which was absent in the parent cells (data not shown).

*Immunoblot analysis*

The HSV1-TK expression in resuscitated HEK293TK+ and HEK293 cells and xenograft tissues was tested by immunoblot analysis. Proteins from cell cultures or xenograft lysates were separated by 10% SDS-polyacrylamide gel electrophoresis according to standard protocols (Bio-Rad) at 100 V for 90 min and transferred onto a PVDF blotting membrane at 60 mA for 90 min. The blots were blocked in 5% dried milk in Tris-buffered saline-Tween-20 (TBS-T) and processed for immunostaining with a rabbit anti-HSV1-TK polyclonal antibody (1:500, Santa Cruz Biotechnology) or a rabbit anti-actin antibody (1:8000, Sigma) over night at 4°C. After washing with TBS-T, the membranes were incubated with rabbit anti-goat IgG Peroxidase Conjugate (Sigma-Aldrich) for 1 h at room temperature. The antigen–antibody complexes were detected by enhanced chemoluminescence (ECL, Amersham, Buckinghamshire, UK).

*Animals*

Animal studies were approved by the Veterinary Office of Canton Zurich and complied with Swiss laws and guidelines on animal protection and husbandry. Subcutaneous xenografts were produced in 7 weeks old female NMRI nude mice (Charles River, Sulzfeld, Germany) by subcutaneous injection in the shoulder region of 5 x $10^6$ cells in 100 μL PBS, pH 7.4, under 2-3% isoflurane (Abbott) anesthesia. Transgenic HEK293TK+ cells were injected on the left side, control HEK293 (HEK293 control) cells on the right side. Xenograft growth and body weight were monitored regularly. Experiments were conducted when the xenografts reached a vol-

ume between 1 and 2 $cm^3$, 3-4 weeks after subcutaneous inoculation.

*In vitro phosphorylation of FHOMP*

Phosphorylation of FHOMP, penciclovir (PCV) a well known substrate for HSV1-TK but not the human TK (hTK) and deoxythymidine (dT; positive control to assess the functionality of both HSV1-TK and human TK, hTK) by HSV1-TK and hTK were monitored by HPLC as described previously [20]. In brief, 1-5 mM substrate were incubated with 3 μg of HSV1-TK or hTK and 5 mM ATP in a buffer solution (pH 7.4) at 37 °C and quenched after 20 and 60 min. The recombinant enzymes, HSV1-TK and hTK, were expressed and purified according to a previously published protocol [21]. The formation of adenosine-diphosphate (ADP) was monitored. A blank reaction (without substrate) was run concurrently to account for substrate-independent ATP hydrolysis.

*Accumulation of [$^{18}$F]FHOMP in HEK293TK+, HEK293 control and murine P388 cells*

Uptake of [$^{18}$F]FHOMP and [$^{18}$F]FHBG into HEK293TK+, HEK293 control and P388 cells was determined according to a previously published protocol [20]. In brief, cells were incubated in a 12-well culture plate with 1 mL medium containing 130 kBq [$^{18}$F]FHOMP or [$^{18}$F]FHBG per well. The radioactivity of the cell lysate and the combined incubation medium and washing solutions, respectively, were measured in a gamma counter (Wizard, Perkin Elmer) at the indicated time points. Radioactivity of the cell lysates was normalized to total protein determined in 50 mL cell lysate with the *DC*™ Protein Assay Kit I (Bio Rad, Hercules CA). Cell uptake was calculated as the percent accumulated radioactivity per mg protein ((dpm cells x 100 / (dpm cells + dpm medium))/mg protein) and corresponding uptake ratios between HEK293TK+ or P388 and HEK293 control cells were calculated [22].

*In vitro metabolism with liver microsomes*

[$^{18}$F]FHOMP metabolism by microsomal enzymes was investigated *in vitro* employing pooled mouse or human liver microsomes (BD Biosciences). The test compound (17 MBq) or 34 μM testosterone (positive control), was preincubated for 5 min with NADPH regenerating system (NADPH-RS; BD Biosciences) according to the manufacturers protocol in 0.1 M phosphate buffer (pH 7.4) at 37 °C before addition of the microsome suspension (0.5 mg protein per mL). A suspension of microsomes without NADPH-RS and a suspension of NADPH-RS without microsomes were used as negative controls. At different time points (0, 10, 20, 60, 90, and 120 min) 100 mL samples were withdrawn and the enzymatic reactions were stopped and proteins precipitated with an equal volume of ice-cold acetonitrile. Samples were centrifuged at 13200 rpm for 3 min to obtain the supernatant which was filtered (0.45 μm), and diluted 1:1 with 0.05 M sodium phosphate buffer (pH 7.0) to be analyzed by Waters ACQUITY UPLC® system as described. Samples of the formulated solution in water containing 5% ethanol and stored at room temperature were used to check for chemical decomposition.

*Blood radioactivity-time curve and biological half-life of [$^{18}$F]FHOMP*

To estimate the biological blood half-life of [$^{18}$F]FHOMP, three mice (female NMRI nude mice, 21-25 g; Charles River) were injected into a lateral tail vein with 9-12 MBq [$^{18}$F]FHOMP in 100 μL saline containing maximal 5% ethanol. Blood samples were drawn through the contra-lateral tail vein at several time points from 2 to 120 min after injection. The radioactivity in each blood sample was measured with a gamma counter (Wizard, Perkin Elmer), corrected for radioactivity decay and the percentage of injected dose per g blood (%ID/g) was calculated and plotted against the time point of blood withdrawal. Radioactivity-time curves were fitted with a mono-exponential function $\%ID/g(t)=\%ID/g(0)\times e^{kt}$, where %ID/g(0) is the fitted starting blood radioactivity at time 0, k is the rate constant in $min^{-1}$ and t the time in min. Biological half-life values were calculated as $t_{1/2}=\ln 2/k$.

*Small-animal PET*

Xenograft bearing mice (21-30 g) were administered 17-24 MBq [$^{18}$F]FHOMP (n = 5) or 7-25 MBq [$^{18}$F]FHBG (n = 5) in 100 μL saline containing ≤ 5% ethanol via tail vein injection. Anesthesia was induced with 2-3% isoflurane (Abbott) in air-oxygen 5 min prior to PET/CT acquisition. Depth of anesthesia and tempera-

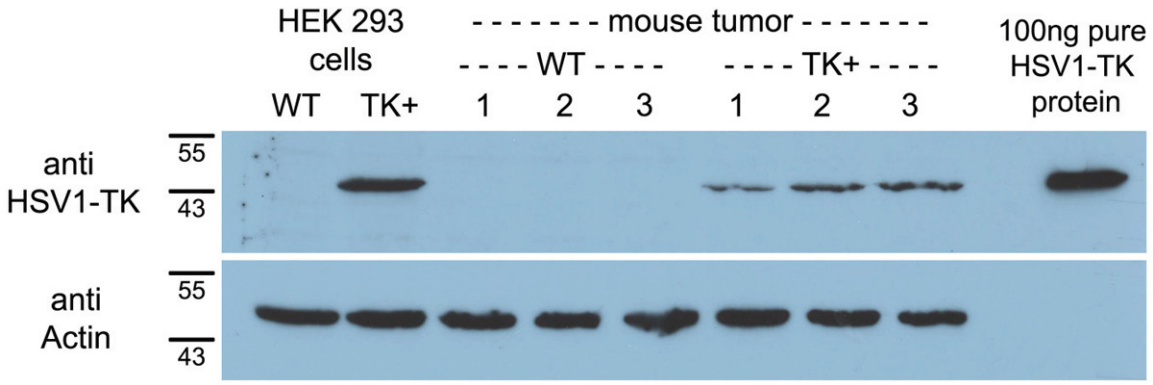


**Figure 2.** Western blot analysis of HSV1-TK expression in transfected (TK+) and nontransfected control (WT) cells (HEK293) and xenograft tissues (tumor) using anti-HSV1-TK polyclonal antibody. Purified HSV1-TK protein served as positive control. Actin expression verified that the same amount of protein was loaded per lane.

ture were controlled as described previously [23]. PET/CT scans were performed with a GE VISTA eXplore PET/CT tomograph with an axial field of view of 4.8 cm [24]. Dynamic (one bed position, list mode) and static (two bed positions, 15 min upper body followed by 15 min lower body) scans were acquired over 90 and 30 min, respectively. Data were reconstructed by 2D ordered-subset expectation maximization (2D OSEM), dynamic scans were reconstructed into 5 min time frames. Region of interest analysis was conducted with the software PMOD 3.2 (PMOD, Switzerland). Volumes of interest (VOIs) were drawn according to the CT images and the average background activity was estimated from a sphere with a volume of ca 0.5 $cm^3$ between the two xenografts. Standardized uptake values (SUVs) were calculated from the VOI average activities per $cm^3$ multiplied with the body weight (with 1 g corresponding to 1 $cm^3$) and divided by the injected activity dose (all decay corrected).

*Ex vivo biodistribution studies of [$^{18}$F]FHOMP and [$^{18}$F]FHBG*

To perform *ex vivo* biodistribution studies of [$^{18}$F]FHOMP and [$^{18}$F]FHBG, HEK293 control and HEK293TK+ xenograft bearing nude mice (25-30 g) were administered 4.7-5.1 MBq [$^{18}$F]FHOMP (n = 4) or 4.5-5.0 MBq [$^{18}$F]FHBG (n = 3) in 100 µL saline containing ≤5% ethanol via tail-vein injection. Animals were sacrificed and dissected 60 min after injection, organs and tissue samples were weighed and the radioactivity determined in a gamma counter. The time point of dissection was chosen according to dynamic PET scans and at a time-point when [$^{18}$F]FHOMP activity ratios between HEK293TK+ and control xenografts were highest. Decay corrected radioactivity was expressed in analogy to the SUV as the ratio between the detected activity per gram tissue and the injected dose per gram body weight ($SUV_{biodis}$).

*Effect of ENT1 inhibition on [$^{18}$F]FHOMP PET and ex vivo biodistribution*

Four mice (19-23 g) received each 15 mg/kg ENT1 inhibitor nitrobenzylmercaptopurine ribonucleoside phosphate (NBMPR-P; generously provided by Dr. Wendy Gati, Department of Pharmacology, University of Alberta, Edmonton Canada) dissolved in aqua ad injectabilia via intraperitoneal injection. At this dosage, NBMPR-P inhibits ENT1 with no observed animal toxicity [25]. One hour after NBMPR-P administration, [$^{18}$F]FHOMP (4.0-6.4 MBq) was injected in 100 mL water containing maximal 5% ethanol via a lateral tail vein. At 60 min after radiotracer injection, three animals were sacrificed by decapitation under isoflurane anesthesia. Organs and tissues were removed and the accumulated radioactivity was measured in the gamma-counter and expressed as described before. A static whole body PET scan from 60-90 min was acquired with one mouse according to the Section Small-animal PET.

## Results

*Cell line and xenograft characterization*

The HEK293TK+ cell line and HEK293TK+ xenograft tissue showed an intense immunore-

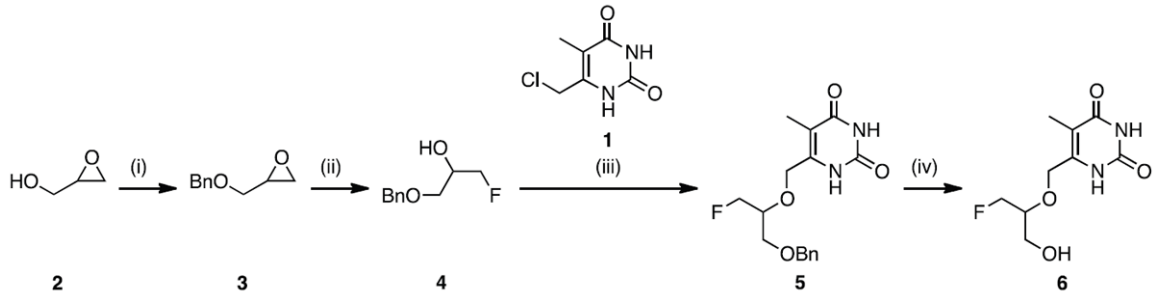

**Figure 3.** Synthesis of reference FHOMP (**6**): (i) NaH, BnBr, THF; (ii) TBABF-KHF$_2$, heptane, 128 °C; (iii) NaH, 6-(chloromethyl)-5-methylpyrimidine-2,4(1*H*,3*H*)-dione, THF, reflux; (iv) 10% Pd/C, $H_2$, MeOH, reflux.

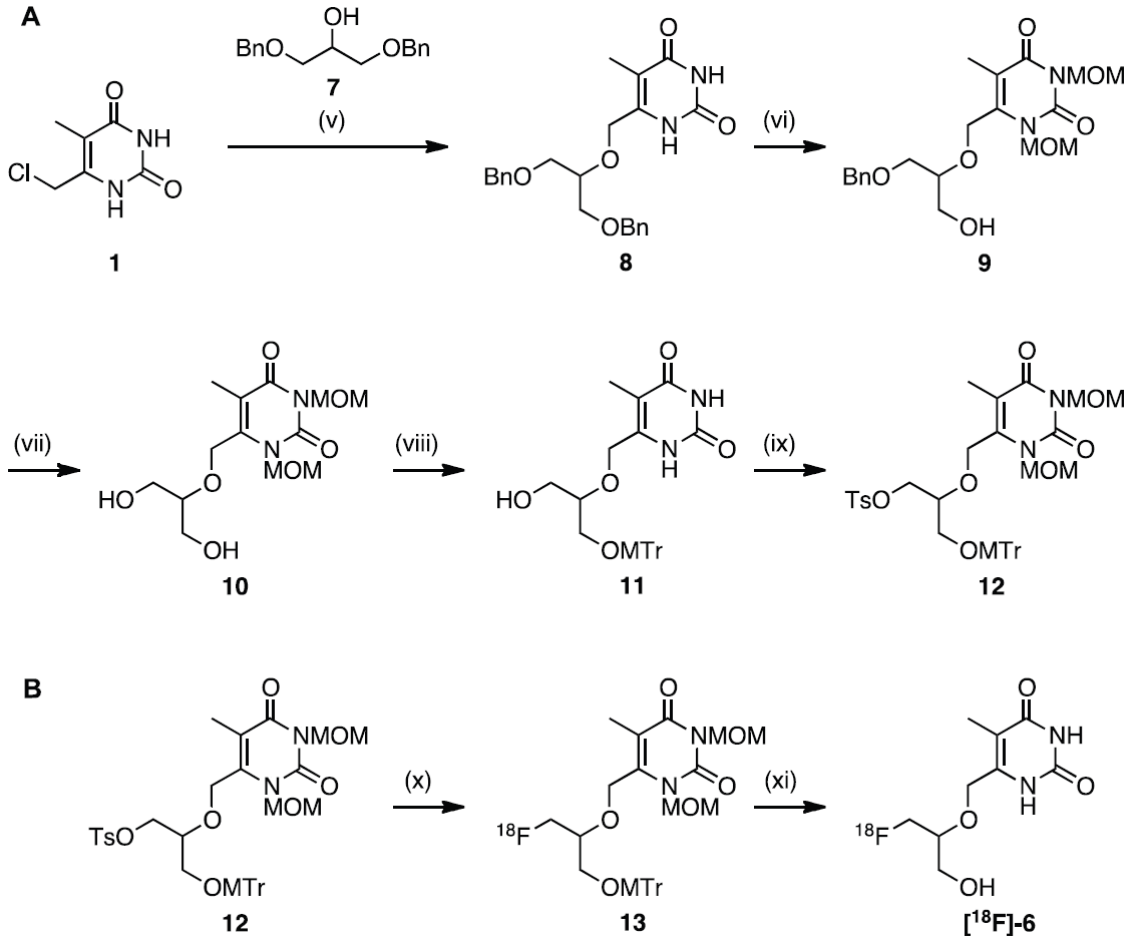

**Figure 4.** A. Synthesis of tosylate precursor **12**: (v) **7**, NaH, THF, reflux; (vi) 1. TMSCl, DIPEA, DCM; 2. MOMCl; (vii) $Pd(OH)_2$, cyclohexene, EtOH, reflux; (viii) MTrCl, TEA, DMAP, DMF; (ix) TsCl, DMAP, pyridine, 30 °C; B. Radiosynthesis of [$^{18}$F]FHOMP ([$^{18}$F]-**6** ): (x) [$^{18}$F]TBAF, *tert*-butanol/ACN 4:1, 110 °C; (xi) conc. HCl, 110 °C.

active band for HSV1-TK protein located at 45 kDa by Western Blot analysis (**Figure 2**). Purified HSV1-TK protein (see above) served as positive control. The HEK293 control cells and HEK293 control xenograft tissue did not show this band.

*Syntheses of reference FHOMP (6) and precursor 12*

The synthesis of reference compound **6** started from glycidol **2** (**Figure 3**) which was trans-

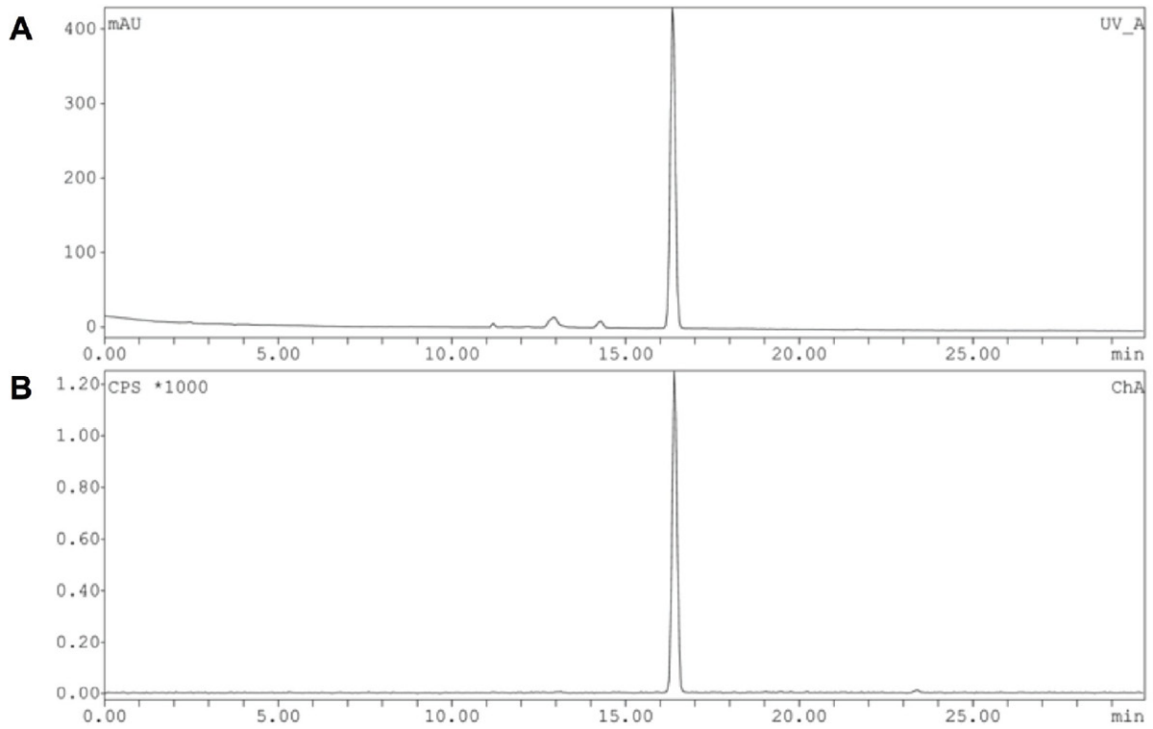


**Figure 5.** HPLC profile of [$^{18}$F]FHOMP ([$^{18}$F]-**6**) after semi-preparative HPLC purification. A. UV absorption at 254 nm: co-injected non-radioactive FHOMP (**6**). B. radio chromatogram: radioactive trace of [$^{18}$F]FHOMP ([$^{18}$F]-**6**).

formed to benzyloxy fluoropropanol 4 in 44% yield as reported previously [26, 27]. Alcohol **4** was reacted with pyrimidine **1** which was synthesized according to a published method [28] to yield benzylated compound **5** in 46%. Deprotection of the benzyl group in **5** was achieved by treatment with Pd/C and hydrogen to afford target compound **6** in 50% yield.

For the synthesis of the precursor (**Figure 4A**), pyrimidine **1** was reacted with dibenzylated alcohol **7** in THF using NaH as a base to afford compound **8** in 49% yield. Treatment of **8** with $Me_3SiCl$ and DIPEA and subsequent reaction with MOMCl in analogy to a published procedure [29] gave N-1 and N-3 protected pyrimidine **9** in 97% yield. Pyrimidine **9** was debenzylated by *in situ* transfer-hydrogenation with $Pd(OH)_2$ on carbon and cyclohexene to yield diol **10** in 93%. Diol **10** was treated with methoxytritylchloride (MTrCl) to afford MTr-protected alcohol **11** in 30% yield. The tosylate precursor **12** was obtained in 45% yield after reacting MTr-protected alcohol **11** with tosylchloride.

*Radiosynthesis of [18F]FHOMP ([18F]-6)*

Tosyl precursor **12** was directly labeled with [$^{18}$F] via nucleophilic substitution using [$^{18}$F] TBAF followed by acidic cleavage of the protecting groups (**Figure 4B**). The [$^{18}$F]-fluorination was performed in *tert*-butanol and acetonitrile (4:1) at 110 °C for 30 min to afford [$^{18}$F]-labeled intermediate **13**. The incorporation yield was 88% by radio-UPLC analysis. The second step involving the acidic hydrolysis of intermediate **13** gave the final compound, [$^{18}$F]-**6**, in 51% radiochemical yield after semi-preparative HPLC purification. Starting from 28-86 GBq, [$^{18}$F]-**6** was typically obtained in a concentration of 1.5-3.6 GBq/mL. The overall decay corrected radiochemical yield was 25%. Quality control by analytical radio-HPLC showed that the radiochemical purity was always greater than 95%. The total synthesis time after end of bombardment (EOB) was about 110 min and the identity of [$^{18}$F]FHOMP was confirmed by co-injection of the non-radioactive reference compound FHOMP (**Figure 5**).

*In vitro phosphorylation of FHOMP*

The selectivity of FHOMP for HSV1-TK over hTK was investigated *in vitro* in a phosphorylation assay with the purified recombinant enzymes. Both recombinant enzymes were functional as indicated by the formation of phosphorylated

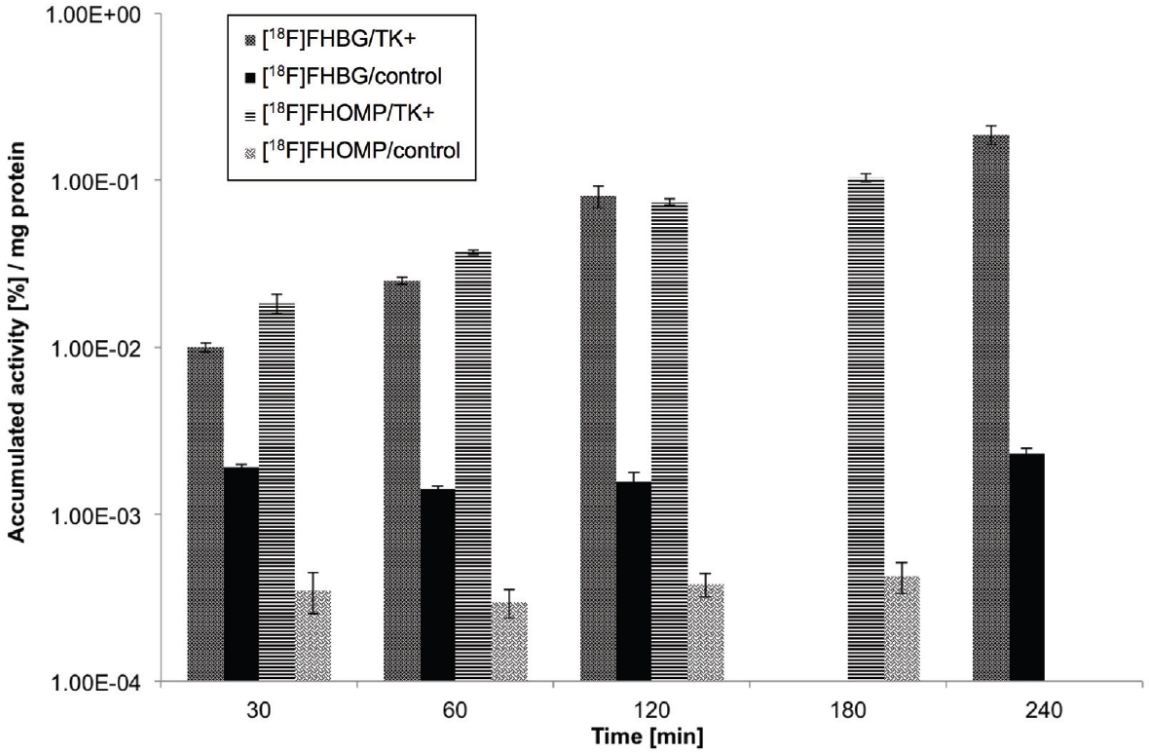


**Figure 6.** *In vitro* uptake (%/mg protein) of [$^{18}$F]FHOMP and [$^{18}$F]FHBG in HEK293TK+ cells (TK+) over HEK293 control cells (control). Data are expressed as mean±standard deviation of triplicate sample. [$^{18}$F]FHBG data has been shown before in [20].

dT (dT-mP) and ADP after incubation with dT. Increasing ADP concentrations were observed during FHOMP and PCV-control incubation with HSV1-TK and ATP but only autohydrolysis was detected with hTK. These data indicate that FHOMP is indeed a substrate for HSV1-TK but not for hTK (Figure S1, Supplementary).

*In vitro cell uptake studies*

**Figure 6** summarizes the uptake of [$^{18}$F]FHOMP and [$^{18}$F]FHBG *in vitro* in HSV1-*tk* transfected (HEK293TK+) and control cells. Cells were incubated for the indicated durations with [$^{18}$F]FHOMP or [$^{18}$F]FHBG. The uptake of [$^{18}$F]FHOMP was 52-fold (at 30 min) and 244-fold (at 180 min) higher in HSV1-TK containing HEK293TK+ cells than in control cells. The uptake ratios for [$^{18}$F]FHBG at 30 min and 240 min were 5 and 81, respectively. Uptake into control HEK293 cells was low for [$^{18}$F]FHOMP with 3.6E-04±7.7E-05 %/mg protein and 1.8E-03±1.3E-04 %/mg protein for [$^{18}$F]FHBG. [$^{18}$F]FHOMP uptake ratios were significantly ($P < 0.02$; Student *t* test) higher than [$^{18}$F]FHBG uptake ratios, i.e., 9.9-fold higher at 30 min, 7.1-fold higher at 60 min, and 3.6-fold higher at 120 min. Uptake of [$^{18}$F]FHOMP into murine P388 cells was lower than into HEK293 control cells, excluding [$^{18}$F]FHOMP accumulation by murine TK or a murine transporter (data not shown).

*Octanol/buffer logD of [$^{18}$F]FHOMP and [$^{18}$F]FHBG at pH 7.4*

The lipophilicity of [$^{18}$F]FHOMP and [$^{18}$F]FHBG was determined by the shake-flask method at physiological pH 7.4. A log $D_{pH7.4}$ of -0.87±0.03 was obtained for [$^{18}$F]FHOMP and -0.87±0.01 for [$^{18}$F]FHBG, respectively.

*In vitro metabolism by liver microsomes*

In mouse or human liver microsomes, over 99% of [$^{18}$F]FHOMP was still intact after 120 min of incubation at 37°C. A stability study of the formulated solution (5% ethanol in water) revealed no radioactive degradation products of the parent compound at room temperature over 240 min.

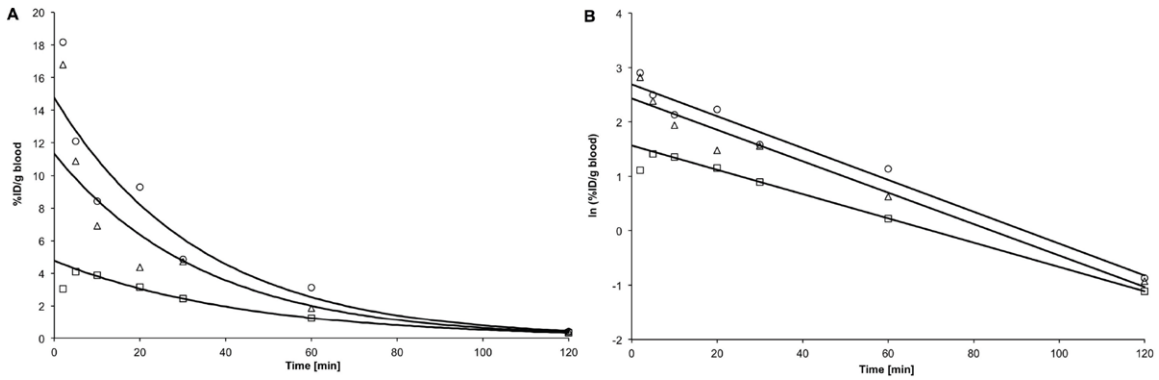


**Figure 7.** Decay-corrected blood radioactivity-time curves after i.v. injection of [$^{18}$F]FHOMP. Linear (A) and semi-logarithmic (B) representations of decay-corrected radioactivity (%ID per g blood) after intravenous injection of [$^{18}$F]FHOMP. Symbols represent the data of three mice, solid lines are fitted mono-exponential functions (weighted for the squared deviations in the ln plot). The first data point (2 min) of the second animal (squares) was excluded from the fit. Fitted biological half-lifes were 23.6 min (circles), 31.1 min (squares), and 24.0 min (triangles).

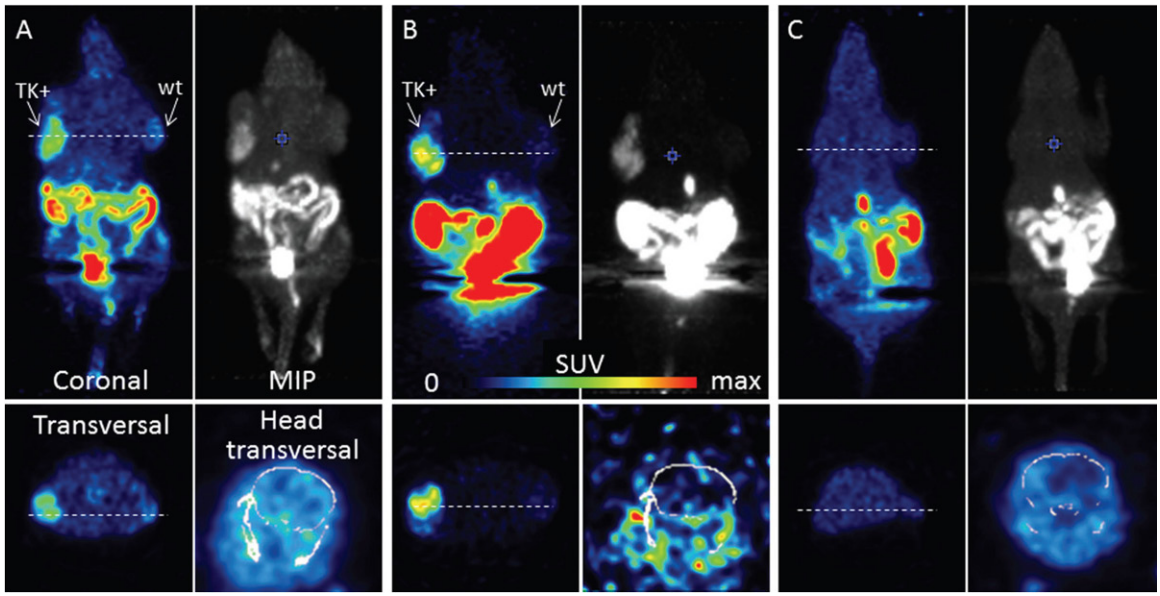


**Figure 8.** PET images of [$^{18}$F]FHOMP and [$^{18}$F]FHBG. Mice were scanned for 30 min (2 bed positions) 60 min after tracer injection. (A) and (B) HSV1-TK+ (left shoulder) and control (right shoulder) xenograft-bearing mice were injected with 12 MBq [$^{18}$F]FHOMP (A) or 21 MBq [$^{18}$F]FHBG (B). C. Mouse without xenografts after ENT-1 blockade with NBMPR-P and injection of 18 MBq [$^{18}$F]FHOMP. Max SUV 1 except for brain sections with max SUV 0.5 (A) and (B) and 0.1 (C). MIP, maximal intensity projections. Anesthesia: 2-3% isoflurane in air/oxygen.

*Blood radioactivity-time curve and biological half-life of [$^{18}$F]FHOMP*

The averaged blood radioactivity-time curves after intravenous injection of [$^{18}$F]FHOMP in three nude mice, uncorrected for potential radiometabolites, are shown in **Figure 7**. The decay-corrected blood radioactivity (%ID/g) decreased with first order kinetics. The radioactivity-time curves were fitted with a mono-exponential function and biological half-life values ($t_{1/2}$) were calculated as described under Methods. The average $t_{1/2}$ was 26.2 ± 4.2 min.

*Small-animal PET studies with [$^{18}$F]FHOMP and [$^{18}$F]FHBG*

Static whole body (two beds, 60-90 min) PET images of xenograft-bearing mice after i.v. injection of [$^{18}$F]FHOMP and [$^{18}$F]FHBG are shown in **Figure 8**. The time frame for the static PET scans was based on the dynamic scans

**Table 1.** Biodistribution ($SUV_{biodis}$) and PET data ($SUV_{PET}$) of [$^{18}$F]FHOMP and [$^{18}$F]FHBG in xenograft-bearing mice and of [$^{18}$F]FHOMP in normal mice injected with the ENT1 blocker NBMPR-P (1h before radiotracer) at 60 min after radiotracer injection

| Tissue | [$^{18}$F]FHOMP | | [$^{18}$F]FHBG | | [$^{18}$F]FHOMP+NBMPR-P | |
|---|---|---|---|---|---|---|
| | $SUV_{biodis}$ | $SUV_{PET}$ | $SUV_{biodis}$ | $SUV_{PET}$ | $SUV_{biodis}$ | $SUV_{PET}$ |
| Xenograft TK+ | 0.34±0.02 | 0.28 | 0.20±0.08 | 0.27 | | |
| Xenograft control | 0.19±0.06 | 0.16 | 0.067±0.00 | 0.07 | | |
| Blood | 0.16±0.03 | | 0.034±0.00 | | 0.15±0.06 | |
| Spleen | 0.11±0.01 | | 0.091±0.03 | | 0.08±0.03* | |
| Liver | 0.16±0.01 | | 0.063±0.01 | | 0.12±0.04 | |
| Kidney | 0.33±0.07 | | 0.39±0.12 | | 0.23±0.10 | |
| Lung | 0.13±0.00 | | 0.040±0.01 | | 0.10±0.04 | |
| Bone | 0.19±0.03 | | 0.050±0.10 | | 0.12±0.04 | |
| Heart | 0.14±0.01 | | 0.034±0.01 | | 0.10±0.03 | |
| Brain | 0.099±0.01 | 0.12 | 0.003±0.00 | 0.01 | 0.057±0.02* | 0.07 |
| Stomach w. cont. | 0.12±0.08 | | 0.026±0.01 | | 0.049±0.01* | |
| Intestine w. cont. | 0.71±0.09 | | 1.77±0.02 | | 0.55±0.13* | |
| Pancreas | 0.10±0.03 | | 0.065±0.03 | | 0.079±0.03 | |
| Muscle | 0.13±0.04 | 0.13 | 0.041±0.01 | 0.04 | 0.12±0.05 | 0.12 |
| Thyroid | 0.19±0.05 | | 0.041±0.01 | | 0.11±0.04 | |
| Gallbladder | 0.5 to 2.4 | | 1.8 to 6.2 | | 1.2 to 2.0 | |
| Urine | 14 to 343 | | 120 to 218 | | 14 to 102 | |

$SUV_{biodis}$ data are the mean±standard deviation of four animals for [$^{18}$F]FHOMP, three animals each for [$^{18}$F]FHBG and for [$^{18}$F]FHOMP + NBMPR-P. [$^{18}$F]FHOMP and [$^{18}$F]FHBG radioactivity accumulation was significantly higher in transgenic xenografts than in the control xenografts for [$^{18}$F]FHOMP (P 0.003) and for [$^{18}$F]FHBG (0.04). *Significantly different from values of [$^{18}$F]FHOMP mice ($P \leq 0.03$) (Student t test). $SUV_{PET}$ data are from the PET scans shown in Figure 8.

and was chosen when SUV ratios between HEK293TK+ and HEK293 control xenografts and between HEK293TK+ xenografts and background (region between the xenografts) for [$^{18}$F]FHOMP were highest (data not shown). [$^{18}$F]FHOMP accumulated in the TK-positive xenograft, consistent with the biodistribution results (see next Section). Uptake in the control xenograft was low and similar to background activity. The respective SUVs are shown in **Table 1**. The hottest spot was the abdomen, followed by the gallbladder and the TK-positive xenograft. [$^{18}$F]FHBG showed similar imaging characteristics as [$^{18}$F]FHOMP with a higher abdominal activity, but less intense general background activities.

*Ex vivo biodistribution of [$^{18}$F]FHOMP and [$^{18}$F]FHBG in xenograft-bearing mice*

**Table 1** summarizes the biodistribution data of [$^{18}$F]FHOMP and [$^{18}$F]FHBG in xenograft-bearing mice at 60 min after radiotracer injection. Radioactivity accumulation for [$^{18}$F]FHOMP and [$^{18}$F]FHBG in transgenic xenografts was significantly higher than in the control xenografts ($P < 0.003$ and 0.04, respectively). The uptake ratio of TK+ to control xenograft was 2.0±0.8 for [$^{18}$F]FHOMP (n=4) and 3.0±1.2 for [$^{18}$F]FHBG (n=3), and the respective TK+ xenograft to blood ratios were 2.1±0.4 and 5.9±2.1. Control xenograft to blood ratios for [$^{18}$F]FHOMP and [$^{18}$F]FHBG were 1.1±0.3 and 2.0±0.2, respectively. The distribution patterns of the two tracers were similar, however, [$^{18}$F]FHOMP exhibited higher activities in most tissues except intestines and kidneys.

*Effect of ENT1 inhibition on ex vivo biodistribution and PET with [$^{18}$F]FHOMP*

To determine whether ENT1 affects [$^{18}$F]FHOMP biodistribution and whether ENT1 inhibition results in lower background radioactivity, mice were analyzed by PET and *post mortem* biodistribution after pre-treatment with the ETN1 inhibitor NBMPR-P. As shown in **Figure 8C**, except for a lower brain uptake, no reduction in background radioactivity was observed compared to the baseline PET image. The *ex vivo*

biodistribution after ENT1 inhibition (**Table 1**) showed significantly reduced radioactivity in the brain ($P < 0.002$), spleen ($P < 0.02$), stomach ($P < 0.002$), intestines ($P = 0.03$) and pancreas ($P < 0.02$). In tissues such as muscle and blood, which generally contribute to high background signals in PET images, no reduction in radioactivity accumulation was observed.

## Discussion

Target compound **6** with substrate specificity for HSV1-TK was successfully synthesized in eight steps (**Figure 3**) with chemical yields ranging from 46 to 88%. During the synthesis of tosyl precursor **12**, N-1 and N-3 in the pyrimidine ring were protected with MOM groups in order to avoid intramolecular cyclization between N-1 and the acyclic moiety at the C-6 position of the pyrimidine ring during radiosynthesis. The protection of N-1 and N-3 atoms in the pyrimidine ring was a critical step and quite challenging probably due to the acidic nature of pyrimidine nitrogen atom. Thus, we were delighted when the treatment of compound **8** with methoxymethylchloride successfully resulted in N-1 and N-3 MOM protection of the dibenzylated compound **9** in an excellent yield of 97%. Standard catalytic hydrogenolysis with $H_2$ over Pd/C led to a complete reduction of the double bond in pyrimidine **9**. This over-reduction has been reported for other pyrimidines [30] therefore, an alternative method involving an *in situ* hydrogenation approach using $Pd(OH)_2$ and cyclohexene system was pursued. Using this approach, no reduction of the double bond was observed and almost a quantitative conversion of compound **9** to **10** (93%) was achieved within two hours.

For the radiosynthesis of [$^{18}$F]-**6**, a different synthetic strategy was adapted in order to circumvent a complex multi-step radiosynthesis. This strategy consisted of developing a suitable precursor that would allow the radiosynthesis in a two-step reaction sequence. As such, compound **12** bearing easily cleavable protecting groups and a tosylate leaving group was designed and synthesized in optimal chemical yields. The radiosynthesis of [$^{18}$F]FHOMP (**Figure 4B**) was accomplished in an overall decay corrected yield of 25%. The optimization of [$^{18}$F]-fluorination step showed that [$^{18}$F]TBAF was the best fluorinating agent when compared to K[$^{18}$F]F and Cs[$^{18}$F]F. Addition of *tert*-butanol enhanced the incorporation yields up to 88% and a 10-fold higher overall yield was obtained using [$^{18}$F]TBAF combined with *tert*-butanol and acetonitrile. Enhancing the nucleophilicity of fluoride ions and also the rate of the nucleophilic fluorination through the use of protic co-solvents has been reported previously [31]. Deprotection of the intermediate [$^{18}$F]-**13** was easily achieved with conc HCl. The harsh hydrolysis conditions generated not only the final product but also a more polar unidentified side-product resulting in a 51% radiochemical yield for this step. Formulation of [$^{18}$F]-**6** without the need to evaporate the mobile phase or trapping on a cartridge is a clear benefit. The radiosynthesis is reliable and robust delivering [$^{18}$F]FHOMP in high product amounts suitable for preclinical pharmacological *in vitro* as well as *in vivo* evaluations .

Negligible *in vivo* defluorination is a prerequisite for a good [$^{18}$F]-labeled PET probe as [$^{18}$F]fluoride accumulates in osseous tissue. Cytochrome P450-mediated defluorination of [$^{18}$F]FHOMP was excluded *in vitro* with human and mouse liver microsomes. Indeed, no bone uptake of radioactivity was observed *in vivo* in mice after [$^{18}$F]FHOMP application.

The *in vitro* uptake of [$^{18}$F]FHOMP into the stably transfected HEK293TK+ cells was significantly higher than in control cells (**Figure 6**). [$^{18}$F]FHOMP showed strikingly higher uptake ratios than [$^{18}$F]FHBG due to lower uptake into control cells at all investigated time points. For comparison, the highest uptake ratio of *N*-Me-[$^{18}$F]FHBT, also a C-6 substituted pyrimidine derivative, was 70 at 120 min [20]. Based on these results, we expected a high uptake ratio of TK+ to control xenograft *in vivo*. The *in vivo* studies showed that the average absolute radioactivity in the transgenic xenografts was higher for [$^{18}$F]FHOMP than [$^{18}$F]FHBG. However, [$^{18}$F]FHBG had a more favorable HSV1-TK+ xenograft/background ratio than [$^{18}$F]FHOMP owing to its relatively low tissue activity.

Low background activity of [$^{18}$F]FHBG may be due to more rapid clearance from the blood than [$^{18}$F]FHOMP resulting in increased TK+/blood or TK+/tissue ratios. Considering the higher intestinal radioactivity of [$^{18}$F]FHBG and the significantly lower blood concentration at 60 min postinjection, we speculate that a hepatic transporter may be involved that

excretes [$^{18}$F]FHBG more efficiently into the bile than [$^{18}$F]FHOMP resulting in lower background but higher abdominal activity for [$^{18}$F]FHBG. In this study, the radioactivity uptake of purine derivative [$^{18}$F]FHBG and pyrimidine derivative [$^{18}$F]FHOMP was cleared by both the hepatobiliary and renal pathways resulting in high radioactivity in the abdominal region and in urinary bladder. [$^{18}$F]FFAU, a pyrimidine derivative, however, is known to be favorably excreted via the kidneys [32]. The reduced abdominal background radioactivity of [$^{18}$F]FHOMP may be considered an advantage when compared [$^{18}$F]FHBG.

In general, due to the low lipophilicity of nucleosides and nucleobases, cell uptake depends on specific nucleoside transport proteins in the plasma membrane [33, 34]. Nucleoside transport proteins are encoded by two gene families: *SLC28*, encoding for the CNTs, consisting of three isoforms (CNT1-3), which are $Na^+$-dependent symporters, and *SLC29*, encoding for the ENTs consisting of four isoforms (ENT1-4) which are Na+-independent diffusion-limited channels [35, 36]. We investigated whether ENT1, which is expressed in many mammalian tissues including erythrocytes, brain, vascular endothelium, placenta, heart, liver, lung and colon may contribute to the higher background radioactivity of [$^{18}$F]FHOMP compared to [$^{18}$F]FHBG. Inhibition of ENT1 with NBMPR-P significantly reduced brain uptake of [$^{18}$F]FHOMP, indicating that ENT1 is involved in blood-brain barrier passage of the radiotracer. However, the general background was not reduced by ENT1 inhibition. In addition, [$^{18}$F]FHOMP uptake into murine cells was lower than into HEK293 control cells *in vitro*, excluding a mouse-specific mechanism of cell retention. It will be important in future studies to verify other factors that could have an effect on the background radioactivity of [$^{18}$F]FHOMP.

## Conclusions

An efficient and convenient chemical and radiochemical synthesis of a new C-6 substituted pyrimidine derivative 6-((1-fluoro-3-hydroxypropan-2-yloxy)methyl)-5-methylpyrimidine-2,4(1*H*,3*H*)-dione (FHOMP) for HSV1-TK imaging has been developed and accomplished in yields and purity suitable for *in vivo* studies with PET. [$^{18}$F]FHOMP exhibited higher uptake ratios between HEK293TK+ and HEK293 control cells than [$^{18}$F]FHBG *in vitro* but not *in vivo*. The lower ratio *in vivo* is a consequence of the higher general background radioactivity of [$^{18}$F]FHOMP. ENT1 is an important mediator of [$^{18}$F]FHOMP uptake in brain but does not contribute to the relatively high tissue radioactivity in general. Although the *in vivo* properties of [$^{18}$F]FHOMP do not outperform [$^{18}$F]FHBG with respect to HSV1-TK+ xenograft/background ratio, the reduced abdominal background radioactivity of [$^{18}$F]FHOMP may be considered an advantage.

## Acknowledgments

We thank Cindy Fischer, Dr. Linjing Mu and Dominique Leutwiler for their support and help during *in vitro* studies and Claudia Keller and Petra Wirth for their assistance in the *in vivo* and *ex vivo* experiments. We thank Dr. Svetlana Selivanova, Dr. Thomas Betzel, Dr. Aristeidis Chiotellis and Lukas Dialer for fruitful discussions and sharing radiochemistry and chemistry knowledge. We thank Kurt Hauenstein for technical purification support. We thank Dr. Jason Holland for reading through the manuscript and for his fruitful comments. We would like to thank the Flow Cytometry Laboratory of the Institute for Biomedical Engineering UZH and ETH Zurich for technical support. Financial support for this study was provided by the Swiss Science National Foundation (Project Nr. 31003A_126963).

## Disclaimer of conflict of interest

None.

## Supporting information

Experimental synthetic methods, characterization of all compounds, HPLC chromatographs of phosphorylation assays of FHOMP and control compounds.

**Address correspondence to:** Dr. Simon M Ametamey, Center for Radiopharmaceutical Sciences of ETH, PSI and USZ, Institute of Pharmaceutical Sciences ETH Zurich, Wolfgang-Pauli-Strasse 10, 8093 Zurich, Switzerland. Tel: +41 44 633 74 63; Fax: +41 44 633 13 67

## References

[1] Kang JH and Chung J-K. Molecular-Genetic Imaging Based on Reporter Gene Expression. J Nucl Med 2008; 49: 164S-179S.

[2] Min J-J and Gambhir SS. Molecular Imaging II. Molecular Imaging of PET Reporter Gene Expression. Edited by Semmler W, Schwaiger M. Berlin, Springer, 2008, pp. 277-303.

[3] Alauddin MM and Tjuvajev JG. Radiolabeled nucleoside analogues for PET imaging of HSV1-tk gene expression. Curr Top Med Chem 2010; 10: 1617-1632.

[4] Paproski RJ, Wuest M, Jans H-S, Graham K, Gati WP, McQuarrie S, McEwan A, Mercer J, Young JD and Cass CE. Biodistribution and Uptake of 3′-Deoxy-3′-Fluorothymidine in ENT1-Knockout Mice and in an ENT1-Knockdown Tumor Model. J Nucl Med 2010; 51: 1447-1455.

[5] Yaghoubi SS, Jensen MC, Satyamurthy N, Budhiraja S, Paik D, Czernin J and Gambhir SS. Noninvasive detection of therapeutic cytolytic T cells with 18F-FHBG PET in a patient with glioma. Nat Clin Prac Oncol 2009; 6: 53-58.

[6] Yaghoubi SS and Gambhir SS. PET imaging of herpes simplex virus type 1 thymidine kinase (HSV1-tk) or mutant HSV1-sr39tk reporter gene expression in mice and humans using [18F]FHBG. Nat Protoc 2007; 1: 3069-3074.

[7] Jacobs A, Voges J, Reszka R, Lercher M, Gossmann A, Kracht L, Kaestle C, Wagner R, Wienhard K and Heiss WD. Positron-emission tomography of vector-mediated gene expression in gene therapy for gliomas. Lancet 2001; 358: 727-729.

[8] Alauddin M, Shahinian A, Park R, Tohme M, Fissekis J and Conti P. In vivo evaluation of 2′-deoxy-2′-[18F]fluoro-5-iodo-1-β-d-arabinofuranosyluracil ([18F]FIAU) and 2′-deoxy-2′-[18F]fluoro-5-ethyl-1-β-d-arabinofuranosyluracil ([18F]FEAU) as markers for suicide gene expression. Eur J Nucl Med Mol Imaging 2007; 34: 822-829.

[9] Soghomonyan S, Hajitou A, Rangel R, Trepel M, Pasqualini R, Arap W, Gelovani JG and Alauddin MM. Molecular PET imaging of HSV1-tk reporter gene expression using [18F]FEAU. Nat Protoc 2007; 2: 416-423.

[10] Tjuvajev JG, Doubrovin M, Akhurst T, Cai S, Balatoni J, Alauddin MM, Finn R, Bornmann W, Thaler H, Conti PS and Blasberg RG. Comparison of Radiolabeled Nucleoside Probes (FIAU, FHBG, and FHPG) for PET Imaging of HSV1-tk Gene Expression. J Nucl Med 2002; 43: 1072-1083.

[11] Yaghoubi S, Barrio JR, Dahlbom M, Iyer M, Namavari M, Satyamurthy N, Goldman R, Herschman HR, Phelps ME and Gambhir SS. Human Pharmacokinetic and Dosimetry Studies of [18F]FHBG: A Reporter Probe for Imaging Herpes Simplex Virus Type-1 Thymidine Kinase Reporter Gene Expression. J Nucl Med 2001; 42: 1225-1234.

[12] MacLaren DC, Toyokuni T, Cherry SR, Barrio JR, Phelps ME, Herschman HR and Gambhir SS. PET imaging of transgene expression. Biol Psychiatry 2000; 48: 337-348.

[13] Raić-Malić S, Johayem A, Ametamey SM, Batinac S, De Clercq E, Folkers G and Scapozza L. Synthesis, 18F-Radiolabelling and Biological Evaluations of C-6 Alkylated Pyrimidine Nucleoside Analogues. Nucleos Nucleot Nucl Acids 2004; 23: 1707-1721.

[14] Johayem A, Raić-Malić S, Lazzati K, Schubiger PA, Scapozza L and Ametamey SM. Synthesis and Characterization of a C(6) Nucleoside Analogue for the in vivo Imaging of the Gene Expression of Herpes Simplex Virus Type-1 Thymidine Kinase (HSV1 TK). Chem Biodivers 2006; 3: 274-283.

[15] Anderson CM, Baldwin SA, Young JD, Cass CE and Parkinson FE. Distribution of mRNA encoding a nitrobenzylthioinosine-insensitive nucleoside transporter (ENT2) in rat brain. Mol Brain Res 1999; 70: 293-297.

[16] Lu H, Chen C and Klaassen C. Tissue distribution of concentrative and equilibrative nucleoside transporters in male and female rats and mice. Drug Metab Dispos 2004; 32: 1455-1461.

[17] Griffiths M, Beaumont N, Yao SM, Sundaram M, Boumah CE, Davies A, Kwong FYP, Coe I, Cass CE, Young JD and Baldwin SA. Cloning of a human nucleoside transporter implicated in the cellular uptake of adenosine and chemotherapeutic drugs. Nat Med 1997; 3: 89-93.

[18] Handa M, Choi D-S, Caldeiro RM, Messing RO, Gordon AS and Diamond I. Cloning of a novel isoform of the mouse NBMPR-sensitive equilibrative nucleoside transporter (ENT1) lacking a putative phosphorylation site. Gene 2001; 262: 301-307.

[19] Alauddin MM and Conti PS. Synthesis and Preliminary Evaluation of 9-(4-[18F]-Fluoro-3-Hydroxymethylbutyl)Guanine ([18F]FHBG): A New Potential Imaging Agent for Viral Infection and Gene Therapy Using PET. Nucl Med Biol 1998; 25: 175-180.

[20] Müller U, Martić M, Gazivoda Kraljević T, Krištafor S, Ross TL, Ranadheera C, Müller A, Born M, Krämer SD, Raić-Malić S and Ametamey SM. Synthesis and evaluation of a C-6 alkylated pyrimidine derivative for in vivo imaging of HSV1-TK gene expression. J Nucl Med Biol 2012; 39: 235-246.

[21] Birringer MS, Perozzo R, Kut E, Stillhart C, Surber W, Scapozza L and Folkers G. High-level expression and purification of human thymidine kinase 1: Quaternary structure, stability, and kinetics. Protein Expres Purif 2006; 47: 506-515.

[22] Yaghoubi SS and Gambhir SS. Measuring herpes simplex virus thymidine kinase reporter gene expression in vitro. Nat Protoc 2006; 1: 2137-2142.
[23] Honer M, Bruhlmeier M, Missimer J, Schubiger AP and Ametamey SM. Dynamic Imaging of Striatal D2 Receptors in Mice Using Quad-HIDAC PET. J Nucl Med 2004; 45: 464-470.
[24] Wang Y, Seidel J, Tsui BMW, Vaquero JJ and Pomper MG. Performance Evaluation of the GE Healthcare eXplore VISTA Dual-Ring Small-Animal PET Scanner. J Nucl Med 2006; 47: 1891-1900.
[25] Gati WP and Paterson ARP. Measurement of nitrobenzylthioinosine in plasma and erythrocytes: a pharmacokinetic study in mice. Cancer Chemother Pharmacol 1997; 40: 342-346.
[26] Lipshutz BH, Moretti R and Crow R. Mixed higher-order cyanocuprate-induced epoxide openings: 1-benzyloxy-4-penten-2-ol. Org Synth Coll Vol 1993; 8: 33.
[27] Akiama Y, Fukuhara T and Hara S. Regioselective synthesis of fluorohydrines via S[N]2-type ring-opening of epoxides with TBABF-KHF[2]. Synlett 2003; 10: 1530-1532.
[28] Murray PE, McNally VA, Lockyer SD, Williams KJ, Stratford IJ, Jaffar M and Freeman S. Synthesis and enzymatic evaluation of pyridinium-Substituted uracil derivatives as novel inhibitors of thymidine phosphorylase. Bioorg Med Chem 2002; 10: 525-530.
[29] Heintzelman G, Fang W-K, Keen SP, Wallace GA and Weinreb SM. Stereoselective Total Synthesis of the Cyanobacterial Hepatotoxin 7-Epicylindrospermopsin: Revision of the Stereochemistry of Cylindrospermopsin. J Am Chem Soc 2001; 123: 8851-8853.
[30] Martin JC, Jeffrey GA, McGee DPC, Tippie MA, Smee DF, Matthews TR and Verheyden JPH. Acyclic analogs of 2'-deoxynucleosides related to 9-[(1,3-dihydroxy-2-propoxy)methyl]guanine as potential antiviral agents. J Med Chem 1985; 28: 358-362.
[31] Kim DW, Ahn D-S, Oh Y-H, Lee S, Kil HS, Oh SJ, Lee SJ, Kim JS, Ryu JS, Moon DH and Chi DY. A New Class of SN2 Reactions Catalyzed by Protic Solvents: Facile Fluorination for Isotopic Labeling of Diagnostic Molecules. J Am Chem Soc 2006; 128: 16394-16397.
[32] Alauddin MM, Shahinian A, Park R, Tohme M, Fissekis JD and Conti PS. Synthesis and Evaluation of 2′-Deoxy-2′-18F-Fluoro-5-Fluoro-1-β-d-Arabinofuranosyluracil as a Potential PET Imaging Agent for Suicide Gene Expression. J Nucl Med 2004; 45: 2063-2069.
[33] Baldwin SA, Mackey JR, Cass CE and Young JD. Nucleoside transporters: molecular biology and implications for therapeutic development. Mol Med Today 1999; 5: 216-224.
[34] Cass CE, Young JD and Baldwin SA. Recent advances in the molecular biology of nucleoside transporters of mammalian cells. Biochem Cell Biol 1998; 76: 761-770.
[35] Baldwin S, Beal P, Yao SM, King A, Cass C and Young J. The equilibrative nucleoside transporter family, SLC29. Pflügers Arch Eur J Physiol 2004; 447: 735-743.
[36] Gray J, Owen R and Giacomini K. The concentrative nucleoside transporter family, SLC28. Pflügers Arch Eur J Physiol 2004; 447: 728-734.

## Supporting Information

*Analytic and chromatographic methods*

Pre-coated Merck silica gel 60F-254 plates were used for thin layer chromatography and the spots were detected under UV light (254 nm). Column chromatography was performed using silica gel (0.040-0.063 mm) Fluka; glass column was slurry-packed under gravity. The $^{1}H$, $^{13}C$ and $^{19}F$ NMR spectra were recorded at 23 °C on a Bruker Avance 400 ($^{1}H$, 400 MHz; $^{13}C$, 100 MHz; $^{19}F$, 376 MHz) spectrometer using $CDCl_3$ or DMSO-$d_6$ as the solvent. Chemical shifts (ppm) were determined relative to internal $CHCl_3$ ($^{1}H$, δ 7.24; $CDCl_3$), internal $CDCl_3$ ($^{13}C$, δ 77.0, $CDCl_3$), internal DMSO-$d_5$ ($^{1}H$, δ 2.49; DMSO-$d_6$), or interal DMSO-$d_6$ ($^{13}C$, δ 39.5, DMSO-$d_6$). For $^{19}F$ NMR measurements, $CFCl_3$ was used as the internal standard. Values of the coupling constant, *J*, are given in hertz (Hz). Low-resolution mass spectra (LRMS) were recorded with a Micromass Quattro micro API LC-ESI. High resolution mass spectra (HRMS) were recorded with a Bruker FTMS 4.7T BioAPEXII (ESI).

Analytical radio-high performance liquid chromatography (HPLC) of [$^{18}F$]FHOMP was performed on an Agilent 1100 series HPLC system equipped with a UV multi-wavelength detector and a Raytest Gabi Star detector using a Gina software. [$^{18}F$]FHOMP was analyzed on a reversed-phase column, (Gemini C18, 250 x 4.6 mm, particle size: 5 µm, Phenomenex) using a flow rate of 1 mL/min (UV detection at 267 nm) and a gradient as follows: Eluent A was water, eluent B was acetonitrile. The gradient was from 100% A to 90% A and 10% B at 0-15 min, then isocratic at 90% A from 15-20 min, then to 100% A from 20-21 min followed by 100% A isocratic from 21-25 min.

Semi-preparative radio-HPLC was performed on an HPLC system equipped with a Merck-Hitachi L-6200A intelligent pump, a Knauer variable-wavelength ultraviolet detector and an Eberline radiation monitor. [$^{18}F$]FHOMP was purified on a reversed phase column, (Gemini C18, 250 x 10 mm, particle size: 5 µm, Phenomenex) using a flow rate of 4 mL/min and a gradient as follows: Eluent A was water, eluent B was ethanol. After 10 min isocratic 100% A the gradient was from 100% A to 90% A and 10% B at 10-30 min.

For the determination of the microsomal stability of [$^{18}F$]FHOMP Ultra Performance Liquid Chromatography (UPLC) was performed using a Waters ACQUITY UPLC® system equipped with a Berthold FlowStar LB513 radioactivity flow through detector (coincidence detection) and a Waters ACQUITY UPLC® BEH 2.1 x 50 mm, 1.7 µm $C_{18}$ reversed-phase analytic column. Elution was performed at a flow of 0.6 mL/min and a wavelength of 267 nm with a gradient from 100% A (sodium phosphate buffer, pH 7.0) and 0 % B (acetonitrile) to 90% A and 10% B over a 1.5-min period, then a gradient to 30% A and 70% B until 2 min followed by a constant flow of 30% A and 70% B until 3.0 min, then a gradient to 100% A and 0% B to 3.1 min followed by a constant flow of 100% A until 3.2 min.

*Synthesis of reference FHOMP (**6**)*

**6-(Chloromethyl)-5-methylpyrimidine-2,4(1H,3H)-dione (1)**: Compound **1** was synthesized according to published protocols starting from 5,6-dimethylpyrimidine-2,4(1*H*,3*H*)-dione [1]. $^{1}H$ NMR (400 MHz, DMSO-$d_6$): δ 1.82 (s, 3H, C*H*$_3$), 4.43 (s, 2H, C*H*$_2$), 10.87 (s, 1H, N1*H*), 11.16 (s, 1H, N3*H*) ppm. $^{13}C$ NMR (100 MHz, DMSO-$d_6$): δ 9.1, 39.4, 107.4, 145.3, 150.6, 164.8 ppm. LRMS (ESI+) m/z 174.71 (*M*+H)$^+$.

**2-(Benzyloxymethyl)oxirane (3)**: Compound **3** was prepared by benzylation of (±)-glycidol (**2**) by following published methods [2]. $^{1}H$ NMR (400 MHz, $CDCl_3$): δ 2.62 (dd, 1H, *J* = 5.0, 2.7 Hz, CH-C*H*$_2$-O), 2.80 (dd, 1H, *J* = 4.9, 4.1 Hz, CH-C*H*$_2$-O), 3.19 (m, 1H, CH), 3.45 (dd, 1H, *J* = 11.5, 5.7 Hz, O-C*H*$_2$), 3.72 (dd, 1H, *J* = 14.1, 7.1 Hz, O-C*H*$_2$), 4.60 (dd, 2H, *J* = 23.2, 11.9 Hz, Ph-C*H*$_2$-O), 7.26-7.38 (m, 5H, Ph) ppm. HRMS (ESI+) m/z found 164.0830, calcd 164.0837 for $C_{10}H_{12}O_2$.

**1-(Benzyloxy)-3-fluoropropan-2-ol (4)**: Epoxide **3** was selectively opened via fluorination using TBABF-$KHF_2$ according to published methods [3]. $^{1}H$ NMR (400 MHz, $CDCl_3$): δ 2.54 (bs, 1H, OH), 3.58 (m, 2H, O-C*H*$_2$-CH), 4.05 (m, 1H, O-CH$_2$-C*H*), 4.46 (ddd, 1H, $J_{H,F}$ = 47.5 Hz, $J_{H,H}$ = 18.3, 9.7 Hz, F-C*H*$_2$), 4.48 (ddd, 1H, $J_{H,F}$ = 47.5 Hz, $J_{H,H}$ = 18.3, 9.7 Hz, F-C*H*$_2$), 4.57 (s, 2H, Ph-C*H*$_2$-O), 7.29-7.39 (m, 5H, Ph) ppm. $^{13}C$ NMR (100 MHz, $CDCl_3$): δ 69.3 (d, $J_{C,F}$ = 20.5 Hz), 70.0 (d, $J_{C,F}$ = 6.8), 73.5, 83.9 (d, $J_{C,F}$ = 169.9 Hz), 127.8,

127.9, 128.5, 137.6 ppm. $^{19}$F NMR (376 MHz, $CDCl_3$): δ -232.1 (dt, 1F) ppm. HRMS (ESI+) m/z found 184.0893, calcd 184.0899 for $C_{10}H_{13}FO_2$.

**6-((1-(Benzyloxy)-3-fluoropropan-2-yloxy)methyl)-5-methylpyrimidine-2,4(1H,3H)-dione (5)**: NaH (60% in mineral oil, 39 mg, 1.629 mmol) was added to a solution of **4** (100 mg, 0.586 mmol) in THF (17 mL) at 0 °C. The mixture was stirred for 30 min at room temperature. Compound **1** (55.4 mg, 0.317 mmol) was added at 0 °C and the reaction was stirred for 5 min at 0 °C. After warming to room temperature, the mixture was heated to reflux for 16 h. The reaction was cooled to room temperature, quenched with ice and water, diluted with ethylacetate and washed with water and brine. The organic phase was dried over $MgSO_4$ and concentrated. The residue was purified by column chromatography on silica gel ($CH_2Cl_2$ : $CH_3OH$ = 30 : 1) to afford **5** (46.6 mg, 46%). $^1$H NMR (400 MHz, DMSO-$d_6$): δ 1.75 (s, 3H, C*H*$_3$), 3.57 (dd, 2H, *J* = 5.5, 1.0 Hz, BnO-C*H*$_2$), 3.83 (m, 1H, C*H*), 4.41 (s, 2H, C6-C*H*$_2$), 4.52 (s, 2H, Ph-C*H*$_2$), 4.55 (m, 2H, C*H*$_2$-F), 7.32 (m, 5H, Ph), 10.46 (s, 1H, N1*H*), 11.07 (s, 1H, N3*H*) ppm. $^{13}$C NMR (100 MHz, DMSO-$d_6$): δ 9.0, 65.2, 68.1 (d, $J_{C,F}$ = 8.5 Hz), 72.4, 77.2 (d, $J_{C,F}$ = 18.5 Hz), 82.7 (d, $J_{C,F}$ = 167.4 Hz), 106.0, 127.5, 128.3, 138.0, 145.9, 150.7, 164.9 ppm. $^{19}$F NMR (376 MHz, DMSO-$d_6$): δ -230.1 (dt, 1F) ppm. LRMS (ESI+) m/z 322.68 (*M*+H)$^+$.

**6-((1-Fluoro-3-hydroxypropan-2-yloxy)methyl)-5-methylpyrimidine-2,4(1H,3H)-dione (6)**: Palladium on activated carbon 10% (15 mg, 0.014 mmol Pd) was added to a 10 mL-reacti-vial containing **5** (46.6 mg, 0.145 mmol). Methanol (1 mL) was added and the system was flushed with argon. $H_2$ gas was bubbled into the system using a balloon. Having the system saturated with $H_2$, the balloon was removed and the closed system was heated to 80 °C for 20 h. After cooling to room temperature and filtration through celite ($CH_3OH$) the crude was purified by column chromatography on silica gel ($CH_2Cl_2$ : $CH_3OH$ = 20 : 1) to obtain **6** (17 mg, 50%). $^1$H NMR (400 MHz, DMSO-$d_6$): δ 1.74 (s, 3H, C*H*$_3$), 3.51 (t, 2H, *J* = 10.4 Hz, C*H*$_2$-OH), 3.63 (m, 1H, C*H*), 4.41 (s, 2H, C6-C*H*$_2$), 4.47 (m, 2H, C*H*$_2$-F), 5.02 (t, 1H, *J* = 11.3 Hz, O*H*), 10.40 (s, 1H, N1*H*), 11.04 (s, 1H, N3*H*) ppm. $^{13}$C NMR (100 MHz, DMSO-$d_6$): δ 8.8, 59.4 (d, $J_{C,F}$ = 6.7 Hz), 64.9, 79.2 (d, $J_{C,F}$ = 14.2 Hz), 82.1 (d, $J_{C,F}$ = 133.1 Hz), 105.2, 146.2, 150.6, 164.8 ppm. $^{19}$F NMR (376 MHz, DMSO-$d_6$): δ -230.4 (1F) ppm. HRMS (ESI+) m/z found 233.0932, calcd 233.0932 for $C_9H_{14}FN_2O_4$.

*Synthesis of precursor **12***

**6-((1,3-Bis(benzyloxy)propan-2-yloxy)methyl)-5-methylpyrimidine-2,4(1H,3H)-dione (8)**: NaH (60% in mineral oil, 124.5 mg, 3.11 mmol) was added to a solution of 1,3-bis(benzyloxy)propan-2-ol (**7**) (213 µL, 0.86 mmol) in THF (10 mL) at 0 °C. The mixture was stirred for 60 min at room temperature. A solution of **1** (147.1 mg, 0.84 mmol) in THF (5 mL) was added at 0 °C over 40 min. The reaction was stirred at room temperature for 30 min and heated to reflux for 19 h. After this time, the mixture was concentrated, treated with ice water and neutralized. The solution was extracted with ethylacetate. The combined organic phases were dried over $MgSO_4$ and concentrated. The residue was purified by column chromatography on silica gel ($CH_2Cl_2$ : $CH_3OH$ = 40 : 1) to afford **8** (168.5 mg, 49%) as yellow solid. $^1$H NMR (400 MHz, DMSO-$d_6$): δ 1.72 (s, 3H, C*H*$_3$), 3.55 (m, 4H, BnO-C*H*$_2$), 3.78 (m, 1H, C*H*), 4.43 (s, 2H, C6-C*H*$_2$), 4.50 (s, 4H, Ph-C*H*$_2$), 7.32 (m, 10H, Ph), 10.36 (s, 1H, N1*H*), 11.04 (s, 1H, N3*H*) ppm. $^{13}$C NMR (100 MHz, DMSO-$d_6$): δ 8.8, 65.2, 69.5, 72.2, 77.9, 105.1, 127.4, 127.4, 128.1, 138.1, 146.4, 150.5, 162.7 ppm. LRMS (ESI+) m/z 410.76 (*M*+H)$^+$.

**6-((1,3-Bis(benzyloxy)propan-2-yloxy)methyl)-1,3-bis(methoxymethyl)-5-methylpyrimidine-2,4(1H,3H)-dione (9)**: Compound **8** (65 mg, 0.158 mmol) was dissolved in DIPEA (300 µL) and dichloromethane (450 µL) and the mixture was stirred for 30 min. Chlorotrimethylsilane (60 µL, 0.473 mmol) was added and the reaction was stirred for 30 min. After this time, methoxymethyl chloride (MOMCl) (70 µL, 0.92 mmol) was added. After 1 h, additional MOMCl (250 µL, 3.29 mmol) was added. After 22 h, the reaction was diluted with ethylacetate, washed with saturated aqueous $NaHCO_3$ solution and extracted with ethylacetate. The combined organic phases were combined, washed with brine, dried over $Na_2SO_4$ and concentrated in vacuo. The crude product was purified by column chromatography on silica gel (ethylacetate : hexane = 1:1) to yield **9** (77 mg, 97%). $^1$H NMR (400 MHz, $CDCl_3$): δ 2.01 (s, 3H, C*H*$_3$), 3.34 (s, 3H, N3-MOMC*H*$_3$), 3.43 (s, 3H, N1-MOMC*H*$_3$), 3.57 (m, 4H, BnO-C*H*$_2$), 3.81 (m, 1H, C*H*), 4.52 (s, 4H, Ph-C*H*$_2$), 4.68 (s, 2H, C6-C*H*$_2$), 5.39 (s, 2H, N3-MOMC*H*$_2$), 5.42 (s, 2H, N1-MOMC*H*$_2$), 7.27-

7.37 (m, 10H, Ph) ppm. $^{13}$C NMR (100 MHz, $CDCl_3$): δ 11.1, 57.0, 57.9, 64.4, 70.5, 72.7, 73.7, 75.1, 78.6, 111.9, 127.8, 127.9, 128.5, 137.8, 145.0, 152.5, 163.6 ppm. LRMS (ESI+) m/z 498.80 ($M$+H)$^+$.

**6-(((1,3-Dihydroxypropan-2-yl)oxy)methyl)-1,3-bis(methoxymethyl)-5-methylpyrimidine-2,4(1H,3H)-dione (10)**: To a solution of **9** (300 mg, 0.60 mmol) in ethanol (23 mL), $Pd(OH)_2$ on activated carbon 20% (382.5 mg, 0.54 mmol) and cyclohexene (4.5 mL) were added and the reaction was heated to reflux for 70 min. After cooling, the mixture was filtered through celite (ethylacetate) and the solvent was evaporated to yield **10** (179 mg, 93%) as light-yellow oil. $^1$H NMR (400 MHz, $CDCl_3$): δ 2.09 (s, 3H, C$H_3$), 2.32 (bs, 2H, O$H$), 3.45 (s, 3H, N3-MOMC$H_3$), 3.48 (s, 3H, N1-MOMC$H_3$), 3.62 (m, 1H, C$H$), 3.78 (ddd, 4H, $J$ = 30.2, 11.8, 3.7 Hz, OH-C$H_2$), 4.70 (s, 2H, C6-C$H_2$), 5.41 (s, 2H, N3-MOMC$H_2$), 5.49 (s, 2H, N1-MOMC$H_2$) ppm. $^{13}$C NMR (100 MHz, $CDCl_3$): δ 11.3, 57.5, 58.0, 62.7, 64.0, 72.8, 75.4, 80.8, 112.0, 144.6, 152.4, 163.3 ppm. LRMS (ESI+) m/z 318.70 ($M$+H)$^+$.

**6-(((1-Hydroxy-3-((4-methoxyphenyl)diphenylmethoxy)propan-2-yl)oxy)methyl)-1,3-bis(methoxymethyl)-5-methylpyrimidine-2,4(1H,3H)-dione (11)**: To a solution of **10** (20 mg, 0.063 mmol) in DMF (0.4 mL) triethylamine (9.5 mg, 0.094 mmol) was added and the mixture was stirred at room temperature for 10 min. 4-methoxytritylchloride (20 mg, 0.064 mmol) and catalytic amount of DMAP were added and the reaction was stirred for 2 h at room temperature. The mixture was diluted with ethylacetate, washed with water and brine, dried over $MgSO_4$ and concentrated. The residue was purified by column chromatography on silica gel (ethylacetate : hexane 1:4 to ethylacetate : hexane 1:1) to afford **11** (11.2 mg, 30%). $^1$H NMR (400 MHz, $CDCl_3$): δ 1.95 (s, 3H, C$H_3$), 2.31 (bs, 1H, O$H$), 3.21 (m, 2H, MMTrO-C$H_2$), 3.35 (s, 3H, N3-MOMC$H_3$), 3.36 (s, 3H, N1-MOMC$H_3$), 3.57 (m, 2H, OH-C$H_2$), 3.63 (m, 1H, C$H$), 3.73 (s, 3H, MMTrC$H_3$), 4.57 (dd, 2H, $J$ = 52.6, 11.7 Hz, C6-C$H_2$), 5.34 (m, 4H, MOMC$H_2$), 6.77 (m, 2H, C$H$-C-O-$CH_3$), 7.14-7.36 (m, 12H, MMTrC$H$) ppm. $^{13}$C NMR (100 MHz, $CDCl_3$): δ 11.3, 55.2, 57.5, 57.9, 63.0, 63.5, 64.2, 72.7, 75.3, 80.5, 87.0, 111.8, 113.2, 127.1, 127.9, 128.3, 130.3, 135.1, 144.0, 144.7, 152.4, 158.7, 163.4 ppm. LRMS (ESI+) m/z 612.87 ($M$+H)$^+$.

**2-((1,3-Bis(methoxymethyl)-5-methyl-2,6-dioxo-1,2,3,6-tetrahydropyrimidin-4-yl)methoxy)-3-((4-methoxyphenyl)diphenylmethoxy)propyl 4-methylbenzenesulfonate (12)**: Compound **11** (11.2 mg, 0.019 mmol) was suspended in pyridine (0.3 mL) and stirred at room temperature for 30 min. Tosylchloride (16.4 mg, 0.086 mmol) dissolved in dichloromethane (0.1 mL) was added and the mixture was stirred for 2 h at 30 °C. A catalytic amount of DMAP was added and the reaction was heated at 30 °C for 17 h. The mixture was quenched with water and diluted with ethylacetate. The mixture was washed with 1M $CuSO_4$ solution and extracted with ethylacetate. The combined organic phases were dried over $MgSO_4$ and concentrated. The residue was purified by column chromatography on silica gel (ethylacetate : hexane = 1:1) to obtain **12** (6.4 mg, 45%). $^1$H NMR (400 MHz, $CDCl_3$): δ 1.92 (s, 3H, C$H_3$), 2.44 (s, 3H, TsC$H_3$), 3.21 (d, 2H, $J$ = 19.1 Hz MMTrO-C$H_2$), 3.36 (s, 3H, N3-MOMC$H_3$), 3.43 (s, 3H, N1-MOMC$H_3$), 3.61-3.67 (m, 1H, C$H$), 3.80 (s, 3H, MMTrC$H_3$), 4.03 (dd, 1H, $^2J$ = 10.6, $^3J$ =3.2 Hz , TsO-C$H_2$), 4.10 (dd, 1H, $^2J$ = 10.6, $^3J$ = 3.2 Hz, TsO-C$H_2$), 4.53 (dd, 2H, $J$ = 13.3, 11.7 Hz, C6-C$H_2$), 5.32 (m, 2H, N3-MOMC$H_2$), 5.39 (s, 2H, N1-MOMC$H_2$) 6.81 (m, 2H, S-C-CH-C$H$), 7.21-7.36 (m, 14H, tritylC$H$), 7.74 (m, 2H, S-C-C$H$) ppm. $^{13}$C NMR (100 MHz, $CDCl_3$): δ 11.2, 21.7, 55.2, 57.1, 57.9, 62.5, 64.3, 69.6, 72.7, 75.0, 77.5, 87.0, 112.0, 113.3, 127.2, 127.9, 128.2, 129.9, 130.3, 132.7, 134.8, 143.8, 143.8, 144.3, 145.1, 152.3, 158.8, 163.4 ppm. HRMS (ESI+) m/z found 767.2618 for $[C_{40}H_{44}N_2NaO_{10}S]^+$, calcd 767.2609 for $[C_{40}H_{44}N_2NaO_{10}S]^+$.

*Radiosynthesis of [$^{18}$F]**FHOMP** ([$^{18}$F]-**6**)*

The no-carrier-added [$^{18}$F]-fluoride was trapped on the anion exchange cartridge and directly eluted into a 5-mL sealed reaction vessel using a solution of tetrabutylammonium hydroxide (27.8 mg) in 0.6 mL of methanol. The solvent was removed at 90 °C under reduced pressure and a stream of nitrogen. Subsequently, water was removed by azeotropic distillation with acetonitrile (3 x 1 mL) under reduced pressure and a stream of nitrogen at 90 °C. The vial was kept at room temperature for additional 5 min under vacuum. To this dried [$^{18}$F]TBAF salt was added a solution of the tosylate precursor **12** (4 mg) in 0.3 mL *tert*-butanol and anhydrous acetonitrile (4:1). The reaction mixture was heated for 30 min at 110 °C. After cooling, the crude product was passed through an SPE cartridge (Sep-Pak silica, Waters AG) to

remove TBA and unreacted fluoride. The cartridge was washed with acetonitrile (3 x 0.5 mL). The solvent was evaporated at 90 °C under a stream of nitrogen to dryness. For hydrolysis, 0.6 mL of conc. HCl was added and the mixture was heated for 10 min at 110 °C. The vial was cooled, neutralized with 4 M NaOH (1.5 mL) and diluted with 0.6 M phosphate buffer to a total volume of 5 mL. The crude product was injected onto the semi-preparative radio-HPLC column for HPLC purification. The desired product fraction was collected at approximately 19 min (max. 5% ethanol in water) and directly passed through a sterile filter into a sterile and pyrogen-free vial. Radiochemical yield was determined after purification and based on the amount of starting activity.

*Determination of partition coefficient*

The log $D_{pH7.4}$ of [$^{18}$F]FHOMP and [$^{18}$F]FHBG in 1-octanol/PBS was determined by the shake-flask method as previously described [20]. [$^{18}$F]FHOMP or [$^{18}$F]FHBG (~1.5 MBq) was added in 5 mL water containing 5% ethanol to vials containing 0.5 mL each of 1-octanol and PBS. The vials were shaken for 20 min at room temperature and the phases were separated by centrifugation. The radioactivity was measured in 50 µL of each phase with a gamma counter (Wizard, Perkin Elmer). Measurements were performed in triplicates and log $D_{pH7.4.}$ values were calculated as the logarithmic ratio of the counts in the octanol and PBS samples.

## References

[1] Murray PE, McNally VA, Lockyer SD, Williams KJ, Stratford IJ, Jaffar M and Freeman S. Synthesis and enzymatic evaluation of pyridinium-Substituted uracil derivatives as novel inhibitors of thymidine phosphorylase. Bioorg Med Chem 2002; 10: 525-530.

[2] Lipshutz BH, Moretti R and Crow R. Mixed higher-order cyanocuprate-induced epoxide openings: 1-benzyloxy-4-penten-2-ol. Org Synth Coll Vol 1993; 8: 33.

[3] Akiama Y, Fukuhara T and Hara S. Regioselective synthesis of fluorohydrines via S[N]2-type ring-opening of epoxides with TBABF-KHF[2]. Synlett 2003; 10: 1530-1532.

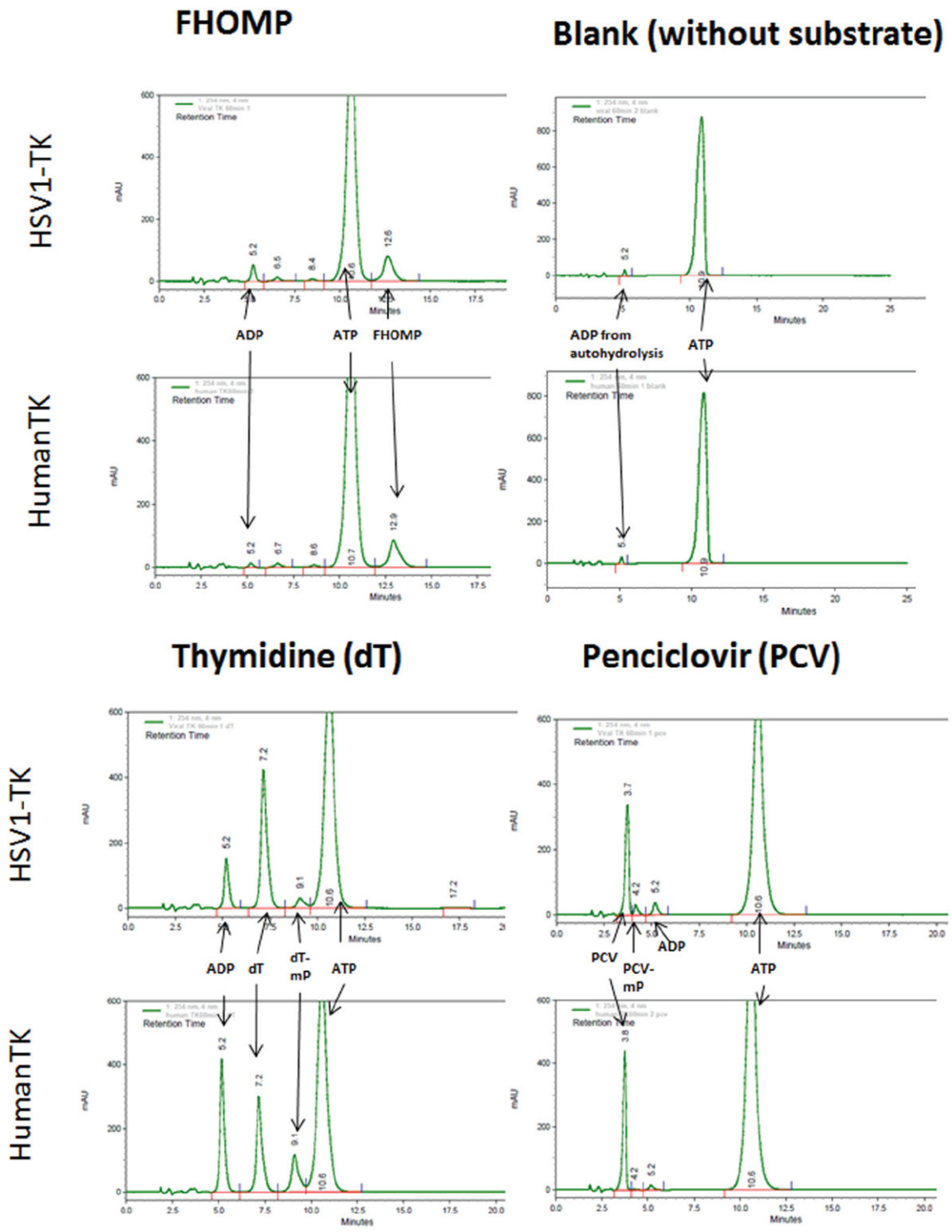


**Figure S1.** Phosphorylation pattern assay at 60 min of incubation: The formation of new peaks (ADP and some monophosporylated compounds) have been monitored by HPLC coupled with a UV detector at 254 nm. To assess the functionality of the HSV1-TK and the human-TK enzymes, thymidine (dT) was used as a positive control. It showed ADP formation for both enzymes as expected and monophosphorylated thymidine (dT-mP) could be detected. Penciclovir was used to compare with a well known HSV1-TK but not human-TK substrate. Very small substrate-independent ATP hydrolysis was observed for the blank (no substrate) for both enzymes. These chromatograms clearly show the formation of ADP for PCV (and some speculated monophosphorylated penciclovir (PCV-mP)) and FHOMP with HSV1-TK but not the human-TK. The data for dT, PCV and blank have been shown before in [20].